Applications of 3D Printing for Formula Student: Optimisation of the Impact Attenuator

Freddie Bickford Smith
Supervisor: Professor Ben Hicks

April 2016

Abstract

The feasibility of manufacture by three-dimensional (3D) printing is investigated for the Formula Student team. The part chosen for study is an impact attenuator, which is mounted inside the car's nose cone, and is required to dissipate kinetic energy in the event of impact while decelerating the car at a safe rate.

Existing research on impact attenuator design was reviewed. The functional requirements, constraints and design objectives of the part were specified. These directed the generation and evaluation of concept designs based on principles of energy dissipation. A multi-layered, absorbent design with variable internal structure was chosen for investigation, with the objectives of minimising mass and material cost. Tensile tests were carried out on specimens of different materials and internal structures. The experimental results were used to screen out unsuitable materials and structures, and to model designs in finite element analysis software.

The final design was compared to a pre-existing part in both numerical simulations and scale-model impact tests. The 3D-printed part performed less well than the foam part, weighed approximately ten times more than the foam part, and incurred a greater material cost. Therefore, this design is not recommended for manufacture. However, further work is recommended in the field of 3D printing energy-absorbent lattice structures made of different materials.

Contents

List of Figures

1 Introduction

This report describes the investigation of the use of 3D printing as a manufacturing process for a racing car part. The background to the problem is outlined, after which a literature review is summarised. This review is used to define the design specification and process. The stages of development are described and discussed, including testing to compare the new design to a pre-existing one. Finally, the findings of the research are discussed, and areas of future work are recommended.

1.1 Project Aim & Objectives

The aim of this research is to investigate the feasibility of designing, making and using 3D-printed parts for Formula Student. This is achieved by completing a series of objectives:

1. Review applications of 3D printing, and select a part to study.
2. Review existing work on the part.
3. Develop a part specification.
4. Generate concept designs, and select one to develop.
5. Devise a development process, and follow it to obtain a final design.
6. Evaluate the final design in comparison to the pre-existing design.

1.2 Formula Student

Formula Student is an annual motorsport competition for universities, run by the Institution of Mechanical Engineers. Teams have the task of designing and building a single-seat, open-wheel racing car, which is tested in competitive events, both static and dynamic. Class 1 is for teams who have made a car with which to compete; Class 2 is for concept designs for future cars [1]. This project will be included in the 2016 Class 2 submission by Bristol Electric Racing, the Formula Student team at the University of Bristol.

1.3 3D Printing

3D printing is a way of making objects by building layer-upon-layer of material. This method of construction enables the manufacture of parts with complex geometries that might be difficult, or impossible, to produce using traditional processes. The process is generally economical with material, with little being wasted. Entry-level machines and the materials they use are relatively low cost.

Parts are printed according to a set of machine instructions generated by software known as a 'slicer', which takes a 3D design file and converts it into a sequence of laminae to be printed. Designs can be changed easily and quickly, and the machinery does not need to be reconfigured between each job.

While the general purpose nature of 3D printers implies adaptability, this comes at the cost of the economies of scale achievable with traditional manufacturing techniques. For this reason, 3D printers have, thus far, been popular for prototyping and DIY projects, as opposed to a widely-used manufacturing process for end products [2]. This research considers whether 3D printing is, in fact, valuable as more than a mock-up tool, and whether it can be used to make meaningfully-improved parts for the Formula Student car.

2 Part Selection

The research began by considering how 3D printing could be best applied to the Formula Student car. Existing work in the fields of 3D printing and Formula Student was reviewed, and an area of focus was chosen.

2.1 Potential Applications

3T RPD, a market-leading 3D printing specialist, has produced a range of components that could be adapted for use in the Formula Student car. Within, a design consultancy, collaborated with 3T to produce a concept design for a heat exchanger, shown in Figure 1a. The part is divided into sub-elements, allowing the overall shape and size to be modified to fit the particular application, as might be necessary in the Formula Student car. The structure is optimised for a high rate of heat transfer, featuring teardrop-shaped internal tubes with flow-disrupting struts, and external cooling fins integrated into the single part. Prototype parts were made by direct metal laser sintering (DMLS), which enabled the manufacture of a part that would likely be impossible to make with traditional processes [3]. A part similar to this could be used to cool the motor and batteries in the Formula Student car.

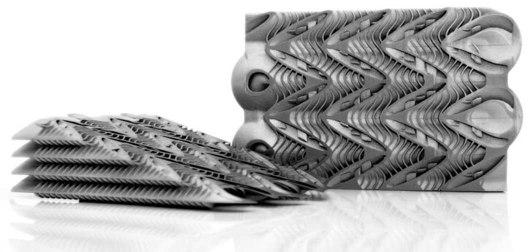

(a) Heat exchanger

(b) Roll hoop

Figure 1: Design concepts developed by Autodesk Within and 3T RPD [3]

Both the Oxford Brookes University Formula Student team and the Jordan-Honda Formula One team have used glass-reinforced plastic to make custom housings for electronic systems in their cars. 3D printing offered low-cost, fast production, in contrast to the process of manufacturing carbon-fibre-reinforced plastic (CFRP) components. The teams found the 3D-printed parts to be stronger and tougher than predicted and required, resulting in better-than-expected life cycles and opportunities for mass reduction. Similarly, Hittech simplified a metal electronics enclosure with integrated cooling channels by manufacturing it by 3D printing rather than using traditional methods. Thermal efficiency was improved, and the complexity, duration and cost of production were reduced [3].

Figure 1b shows a proof-of-concept roll hoop for a racing car, designed by Within using topology optimisation software, and manufactured by 3T RPD. Because the roll hoop is the highest part on a racing car, the objective was to minimise the part's mass, lowering the car's centre of gravity for better handling. The design employs a lightweight titanium lattice structure covered by a thin skin to reduce drag [3]. This concept highlights the potential of using lattice structures to construct strong but lightweight structural parts for Formula Student.

The ability to make parts with complex geometry could be used to develop flexible body parts designed to change shape under load, as shown in Figure 2. Weakened areas in the part could deform elastically under the load exerted by the air flow at a given wind speed, altering the part's aerodynamic profile. Thus, the car could benefit from speed-dependent body part geometry without the need for mechatronic actuators like hydraulic pistons.

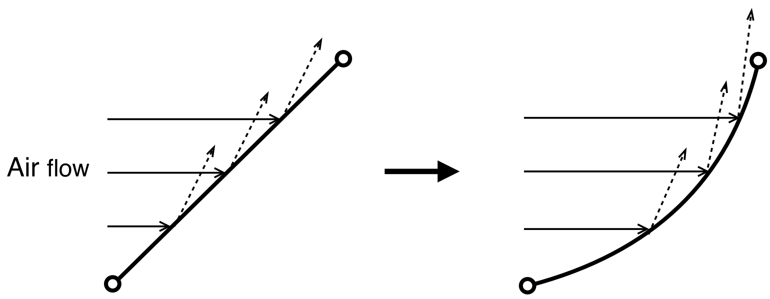

Figure 2: Schematic of a body part with wind-speed-dependent shape

The tyre industry has been conducting extensive research into non-pneumatic tyres, with design similar to that shown in Figure 3a. Without the requirement for a bladder to contain air, there is great scope for enhancing wheel and tyre design to improve performance. Both the internal structure and the external tread could be changed to fit the requirements of the car, giving a greater degree of control over tyre performance than traditional tyres.

The heat exchanger and roll hoop concepts demonstrate the scope for innovation afforded by the ability to manufacture complex internal structures. These principles could be applied to areas of the Formula Student car that absorb impact energy in the event of a crash. One such part is the impact attenuator, a device mounted inside the nose cone that controls the deceleration of the car in a collision by dissipating kinetic energy in a controlled manner (see Figure 3b).

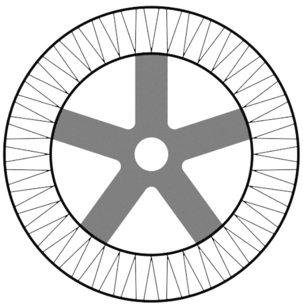

(a) Non-pneumatic tyre

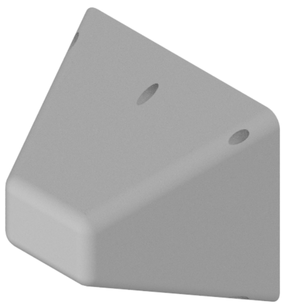

(b) Impact attenuator

Figure 3: Other potential areas of study

To summarise, 3D printing has been shown to be applicable to a range of automotive components. The advantages it offers over traditional manufacturing techniques include the ability to make modular parts with adaptable geometry, the potential to reduce part count by integrating complex features into a single component, and the capacity to build strong but lightweight lattice structures.

2.2 Part Selection

Not all of the potential applications discussed are suitable for this project, in part due to the limitations of the 3D printer and materials used for this research. The machine used is the Makerbot Replicator 2, an affordable desktop machine marketed as a high-quality prototyping machine [4]. It employs 'fused deposition modelling' (FDM) technology, where a computer-controlled print head melts a thermoplastic filament and passes it through a nozzle, depositing material where required. Two machine-compatible materials – polylactic acid (PLA) and a proprietary thermoplastic polyurethane (TPU) trademarked 'Ninjaflex' – are available for use. Given that both materials are thermal insulators, they have no use in the manufacture of a heat exchanger. Study of this part is, accordingly, rejected.

While custom housings are manufacturable with the Replicator 2, the scope of engineering analysis on such simple parts is insufficient for this research. Research into major structural parts, such as the roll hoop, is rejected because it is unlikely that the relatively low-performance plastics being used could feasibly replace high-performance alloys or CFRP. Furthermore, the Formula Student rules prohibit the construction of the roll hoop out of anything but 'a single piece of uncut, continuous, closed section steel tubing' [5].

Because the Bristol Electric Racing team is new to the Formula Student competition, the aerodynamic performance of the car has not yet been analysed. Developing a definitive set of functional requirements for a dynamic body part, operating with the same principle as shown in Figure 2, would be difficult, making the study of this part somewhat arbitrary and not necessarily useful. The application of 3D printing to wheel and tyre design is an area of ongoing research at Bristol Electric Racing. Further research shall not be initiated until existing work is concluded.

Research into the impact attenuator is a suitable area of research given the constraints of machinery and materials: the standard design is made of a polymeric foam, so thermoplastics formed into an alternative structure could potentially satisfy the functional requirements. Selection of the impact attenuator is made more appealing by the opportunity it gives to combine virtual design and simulations with prototyping and experimental testing. Therefore, this part is chosen for further study.

3 Existing Work

The Formula Student organising body provides the design for a standard impact attenuator – a square frustum of Impaxx 700 extruded polystyrene foam [6] – for teams without a custom impact attenuator, as shown in Figure 3b [5]. This fulfils the functional requirements, weighs 0.7kg, and costs $160 to purchase [7]. A similar design constructed from Rohacell 110IG foam was designed and tested by Schormans (2010) for the Formula Student team at Eindhoven University of Technology. The design satisfied the functional criteria with a comfortable margin, so research into less dense foams was recommended [8]. Foster (2015) used a combination of Rohacell foams with varying density to make a lightweight, low-cost, multi-layer impact attenuator [9].

Extensive research has been carried out on aluminium impact attenuators. Boria (2010) conducted an analysis of an impact attenuator constructed from a combination of aluminium sandwich panels and aluminium inner sheets, similar to that shown in Figure 4a. The design fulfilled the functional requirements set out by the Formula Student rules but weighed approximately 3kg [10]. Hart et al. (2010) designed and tested an impact attenuator made of aluminium honeycomb (similar to Figure 4b), and concluded that pre-crushing of the honeycomb would reduce

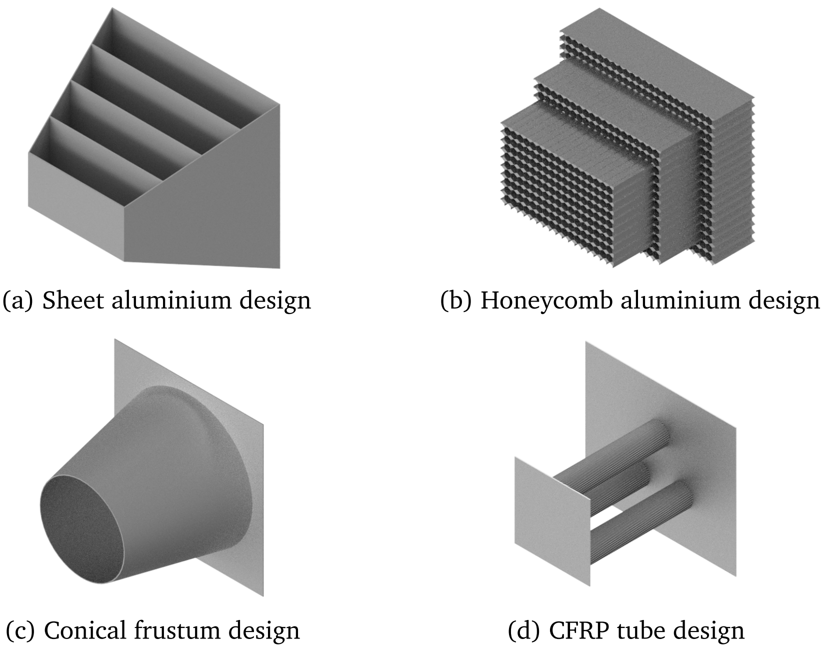

(a) Sheet aluminium design
(b) Honeycomb aluminium design
(c) Conical frustum design
(d) CFRP tube design

Figure 4: Previously-studied impact attenuator designs

the peak deceleration experienced by the car during impact [11].

Oshinibosi (2012) investigated impact attenuators with thin-walled aluminium shell designs, performing a parametric study of the effect of wall thickness and shell shape on crash performance. The conical frustum tube shape (see Figure 4c) was found to offer better specific energy absorption (energy absorbed per unit mass) than the cylindrical tube, square tube and square frustum tube. The conical design was optimised for specific energy absorption, but the functional requirements from the Formula Student rules were not fulfilled [12].

Munusamy & Barton (2010) compared the impact performance of aluminium tubes with and without a core of aramid honeycomb structure. Honeycomb-filled tubes absorbed around 10% more energy than the empty tubes. However, the specific energy absorption was found to be 15% less than for the empty tubes for the same axial deformation in all the test cases [13].

CFRP designs have also been investigated. Wang et al. (2015) found that CFRP cylindrical tubes absorbed impact energy effectively and in a stable manner [14]. Boria & Belingardi (2014) established an accurate method of modelling a CFRP shell impact attenuator with finite element analysis software [15]. Boria & Pettinari (2014) found that CFRP gave greater specific energy absorption than metals when both materials were used to make a square frustrum impact attenuator for an electric vehicle [16]. Similarly, Yang et al. (2012) investigated the behaviour and energy absorption mechanisms of braided CFRP tubes with flexible resin, and found that an impact attenuator comprised of three parallel CFRP tubes (see Figure 4d) provided more stable deceleration than an aluminium box design while weighing less [17].

To summarise, impact attenuators exist in a range of materials and constructions. Lightweight foam impact attenuators, including the standard design prescribed by the Formula Student organising body, have been found to be effective at absorbing kinetic energy in a steady manner. Various aluminium designs have been investigated, but none have been lighter than their foam counterparts. However, CFRP parts offer improved performance and reduced mass compared to all-metal designs.

4 Part Specification

The design process began by setting out the requirements of the part, the constraints on the design and project, and the design objectives for the part. Table 1 summarises the product design specification.

4.1 Functional Requirements

The Formula Student rules state that, attached to a solid steel or aluminium 'anti-intrusion plate' and mounted to the front of a 300kg car travelling at 7m/s, the impact attenuator must give an average vehicle deceleration, a_m, not exceeding $20g$ and peak deceleration, a_p, not exceeding $40g$, where g is gravitational acceleration of 9.81m/s^2. This is equivalent to absorbing 7350J of kinetic energy [5].

Newton's second law can be used to convert the maximum deceleration values into limits for the reaction force provided by the impact attenuator, F_m and F_p:

$$F_m \leq ma_m = 300 \times 20 \times 9.81 = 58,860\text{N}$$
$$F_p \leq ma_p = 300 \times 40 \times 9.81 = 117,720\text{N}$$

where m is the mass of the car in kg. These limits are visualised in Figure 5, which shows sketches of an ideal force-displacement profile and an example of a limiting case profile, both for a hypothetical 200mm-long impact attenuator during a collision. In the ideal case, force rises to approximately 37kN (the lowest-possible value needed to absorb 7350J over a displacement of 200mm), and remains constant, resulting in a minimum average rate of deceleration. In the limiting case, force increases to a peak value, then falls to a steady value, which is maintained until all kinetic energy absorbed (represented by the area under the curve) reaches 7350J at a displacement of around 130mm.

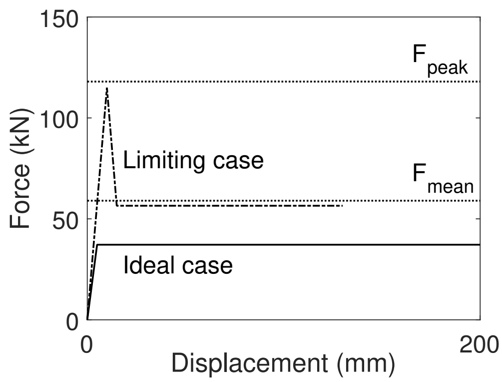

Figure 5: Example force-displacement profiles satisfying the functional requirements

A further requirement of the part is reliability. It is essential that a safety device can be demonstrated to perform consistently to a given standard, ideally in a wide range of operating environments and without degrading over time. This includes performing sufficiently well in off-axis collisions, where the car's fore-aft axis is not perpendicular to the wall it impacts.

4.2 Constraints

The Formula Student rules apply constraints on the size of the part and the method of attachment to the car: the impact attenuator must be at least 200mm long (along the fore/aft axis of the car), 100mm high and 200mm wide; and it must be either welded or bolted to the main chassis [5].

In order to complete the research project within the allotted time period, limits have to be applied to the procedure, reducing the number of experimental variables to a manageable number. Manufacture is limited to the Replicator 2. This machine was chosen because there are multiple available for use, facilitating the manufacture of a large number of specimens. The materials used are PLA and Ninjaflex filaments, which are compatible with the Replicator 2, and are relatively low-cost at approximately £40/kg for PLA [18] and £70/kg for Ninjaflex [19]. The majority of 3D printer settings were kept at the manufacturer's default values.

4.3 Objectives

A key method of improving the performance of a racing car is mass reduction, which improves both acceleration and handling, so this is the primary objective. Another consideration is the cost of the part. In order to allocate more of its budget to key areas of the car, such as the powertrain, it would be beneficial for Bristol Electric Racing to reduce expenditure on the impact attenuator, so cost reduction is another objective. It would also be beneficial to maximise the ability to adapt the shape of the part to the requirements of the rest of the team. This might be most significant when the aerodynamics team proposes a change in the shape and size of the nose cone assembly, to which the impact attenuator belongs.

Functions	Absorb 7350J of kinetic energy
	Mean deceleration less than $20g$
	Peak deceleration less than $40g$
Constraints	Dimensions greater than $200 \times 200 \times 100$mm
	Attachment to anti-intrusion plate and chassis
	Manufacture on Replicator 2 with PLA and Ninjaflex
Objectives	Mass and cost minimisation
	Adaptability of geometry

Table 1: Part specification

5 Design

Energy dissipation mechanisms were researched and translated into impact attenuator concept designs. These were evaluated based on their suitability for this project. A design and its variable parameters were then chosen.

5.1 Energy Dissipation Mechanisms & Concept Designs

Design of the impact attenuator is a challenge in steadily transducing kinetic energy into a different form of energy. One of the principal mechanisms for dissipation of energy is doing work against frictional forces, converting kinetic energy from a macroscopic scale into a microscopic form – internal energy, an increase in which manifests as higher temperature.

Coulomb friction can be generated by making dry surfaces slide over each other. This could be implemented in an impact attenuator by having concentric shells arranged such that their surfaces are in sliding contact during an impact. However, plastic-on-plastic coefficients of friction, μ, tend to be low, with values less than 1 [20]. Since sliding friction force is given by the product of μ and F_N, the force acting perpendicular to the sliding surfaces, low μ values imply that F_N must be large to dissipate lots of energy. This would likely be difficult to implement with reliable off-axis performance: without control of the angle of impact force, the size of the normal component, F_N would vary significantly in different crash scenarios [21].

Motion in liquids gives rise to fluid friction due to viscous effects. This friction could be harnessed by the use of a dashpot – a piston-cylinder device that provides a resistive force proportional to the relative speed of its ends – as in car suspension systems [22]. However, the use of a piston would only be effective if the car impacts an unyielding body at a right angle to the body's surface; off-axis performance would be limited.

Internal friction arises from the interaction between microscopic particles as they move past each other during deformation of material. This effect is present when materials crush or buckle under compressive loads, so can be applied to the design of an impact attenuator by selecting an appropriate material and ensuring that it fails in the desired manner. A salient example of this is the use of polymer foams in bicycle helmets. These cellular materials are characterised by their lower density, stiffness and strength compared to the solid form of the parent material from which they are made. They can undergo large deformations (80-90% strain) at approximately constant ('plateau') stress, making them desirable for decelerating bodies steadily during impacts [23]. The similarity between the stress-strain response of a generic polymer foam (see Figure 6) and the shape of the ideal curve in Figure 5 partly explains why these materials are widely used for energy absorption applications.

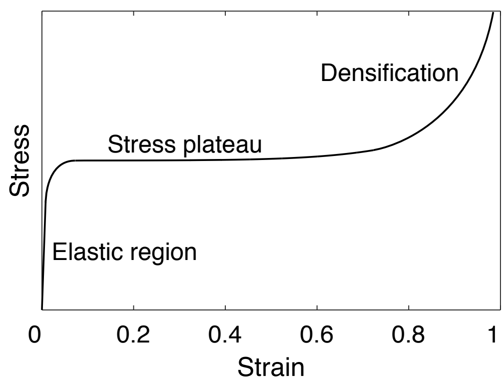

Figure 6: Typical stress-strain for a polymer foam

It is, therefore, evident that cellular materials can offer high performance in energy absorption applications. Research has suggested that there may be potential for improvement, however, with the use of macroscopic lattice structures. Hammetter, Rinaldi & Zok (2013) highlight that, when designed correctly, pyramidal lattice structures can give impressive performance in energy absorption applications, with up to 3-5 times improved specific energy absorption compared to stochastic (random porosity) foams [24]. These structures operate under the same principle as a space frame chassis, where the structure's geometry ensures that forces are transmitted along the axis of struts, loading them in tension or compression rather than bending. The resulting strong, lightweight structures can be effective energy absorbers.

An alternative energy dissipation method is doing work on a material to propagate pre-existing but previously non-catastrophic fractures, ultimately causing brittle failure. Careful design can produce both stable energy absorption and lightweight parts. However, this requires the use of brittle materials with high fracture toughness. Elastomers, such as Ninjaflex, do not exhibit brittle failure, and PLA has fracture toughness values typically less than 25% of that of the CFRP used in Formula One parts [25] [26].

5.2 Chosen Design & Variables

Of the concepts explored, the macroscopic lattice structure was chosen as the most suitable given the manufacturing and material constraints of the project. Furthermore, reviewing the work summarised in Section 3 revealed a gap in the literature in the area of optimising the internal structure of impact attenuators designed to resist load in compression, as opposed to buckling and cracking mechanisms.

With the concept of energy absorption by resistance to plastic deformation chosen, further constraints were applied. The outside shape of the impact attenuator was chosen to be the same as that of the Formula Student impact attenuator. This is a square frustum with maximum dimensions of 250mm long, 350mm wide and 300mm high.

Two ways of splitting up the frustum into layers were considered – one with layers parallel to the front and back faces (Figure 7a); the other with concentric layers (Figure 7b). The former design was chosen because it was proven to work by Foster (2015), and analysis of its simple blocks is more intuitive than calculations on shells. The rationale behind the design is that, assuming that the impact force acts uniformly throughout the part, each layer will require a structure with a different strength because cross-sectional area varies. If those layers requiring less strength can be made of less dense structures, the overall mass of the part could be reduced. However, this may be counteracted by the requirement to have more dense structures in layers requiring high strength.

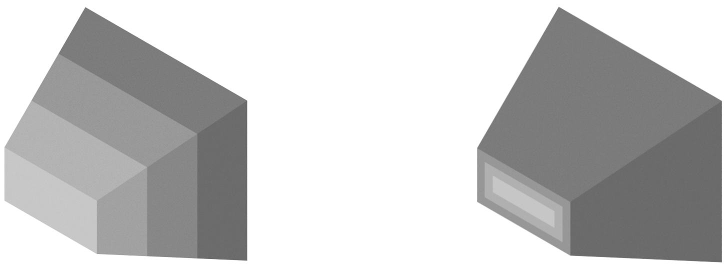

(a) Parallel layer construcion

(b) Concentric layer construcion

Figure 7: Square frustum shape split into multiple layers

Popular slicing packages such as Makerbot Desktop [27] and Slic3r [28] use algorithms to generate so-called ‘infill patterns’ that form the internal structure of 3D-printed objects . Four infill patterns were investigated: Square, Diamond (a 45° rotation of Square), 2D Honeycomb and 3D Honeycomb. These are shown in Figure 8.

The size of the repeating cells that form the infill patterns is determined by the ‘infill density’, expressed as a percentage, where 0% represents a hollow object, and 100% represents a completely

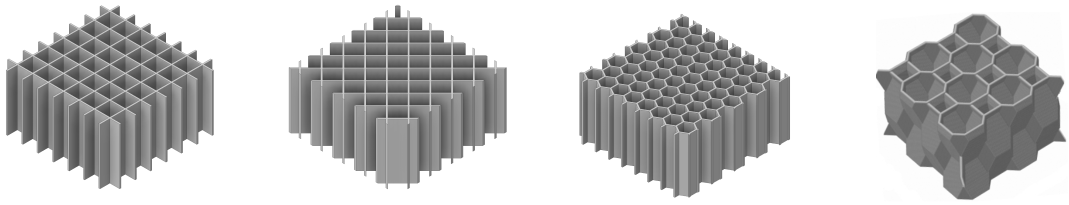

(a) Square (b) Diamond (c) 2D Honeycomb (d) 3D Honeycomb

Figure 8: Infill patterns chosen for study [28]

solid one. Low infill densities (below 25%) were chosen for study in line with the objective of mass reduction.

Typically, a skin is printed on top of the infill structure to create the outside shape described by the design file. Skins were either not used or, when necessary, limited to a single print layer for this study in order to focus on the effect of the internal structure.

Table 2 summarises the design parameters used and the different options for each. Of interest is the relationship between macro-scale (on the scale of the overall part) performance and lower-order meso-scale (infill) and micro-scale (material) variables.

Parameter	**Options**
Material	PLA, Ninjaflex
Number of layers	1, 2, 3, 4, 5
Infill pattern	Square, Diamond, 2D Honeycomb, 3D Honeycomb
Infill density	7%, 14%, 21%

Table 2: Design parameters investigated

6 Characterising 3D-Printed Structures

A major challenge in the development process was identifying a clear relationship between the design parameters and the performance of structures. An empirical approach, consisting of tensile testing, was chosen to find the effective properties of structures made using different materials, infill patterns and infill densities.

6.1 Method

Specimens were manufactured then tested in tension. Force-displacement data was obtained and processed to obtain stress-strain graphs.

6.1.1 Specimens & Apparatus

Specimens were made with outside geometry matching that of the Type I ASTM D638 standard for tensile testing of plastics [29], as shown in Figure 9. Slic3r was used to generate the print files for PLA and Ninjaflex with the four chosen infill patterns and three different infill densities

– 7%, 14% and 21%. These density values were chosen because they ensured that the infill was symmetric along all axes of the specimen. No skin was applied to the main faces of the specimen, leaving the infill visible. A 0.2mm perimeter was used to ensure that the infill cells at the edge of the specimen were closed. 5 specimens were made for each combination of design variables, giving a total of 120 specimens. The average print time per specimen was approximately 10 minutes. The period of specimen manufacture lasted approximately two weeks, in part due to the variable availability of 3D printers, but also because multiple prints either failed or produced poor quality parts.

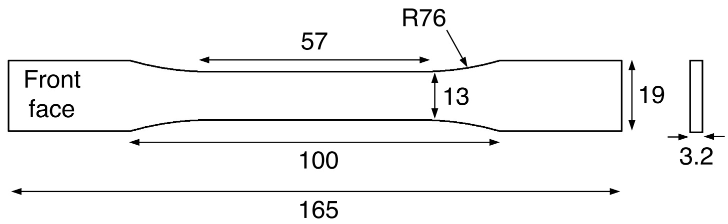

Figure 9: Tensile specimen geometry (mm) from ASTM D638 (Type I)

Tensile testing was carried out on an Instron 3343 1kN machine. The ends of the specimen were clamped by grips, of which one was stationary and one moved on the vertical axis, applying an extension to the specimen that was resisted by an internal reaction force.

6.1.2 Strain Rate

The speed of the moving grip determined the strain rate. Choice of this speed presented a trade-off between experiment duration and the minimisation of strain rate effects on stress-strain response [30]. Preliminary tests were run with a small number of PLA and Ninjaflex specimens at a relatively low strain rate of 10mm/min (suggested by the National Physical Laboratory [31]). These tests were used to identify the approximate extension values at which non-linear behaviour began. For PLA, this extension was 2.5mm; for Ninjaflex, it was 14mm. A low strain rate of 1mm/min was used until these limits of linearity, after which a higher strain rate (10mm/min for PLA; 30mm/min for Ninjaflex) was used. The test was stopped at failure for PLA because this occurred relatively quickly. Ninjaflex specimens experienced very large extensions before failure, so most tests were stopped at an extension of 150mm. At least one repeat test was run for each combination of design parameters. Where manufacture quality was visibly poor, or where force-extension responses were dissimilar between tests, more repeats were run.

6.1.3 Measurement

The displacement of the moving grip from its starting position was output by the testing machine to a computer running data acquisition software. The second output was the force reading of the 1kN load cell connected to the moving grip. Displacement and force were sampled at a frequency of 10Hz. The data sets generated were imported into MATLAB [32] and processed using the script presented in Appendix A, which produced stress-strain plots and found the 0.2% offset yield point and effective modulus for each data set.

In the absence of video extensometers to measure the width of the specimen, the transverse extension – which can be used to calculate transverse strain and, combined with axial strain, Poisson's ratio – could not be measured. The use of vernier callipers to measure width was considered but rejected: the low stiffness of the Ninjaflex specimens resulted in deformation even under small loads, so measurement involving solid contact was unsuitable. In addition, trials carried out on PLA specimens revealed that there was no discernible change in width of these specimens before failure.

6.2 Results

Figures 10 and 11 show combined graphs of selected stress-strain data sets for each infill pattern made of PLA and Ninjaflex respectively. The values obtained for yield stress, σ_y, yield strain, ϵ_y, and effective modulus, E', are given in Appendix A.

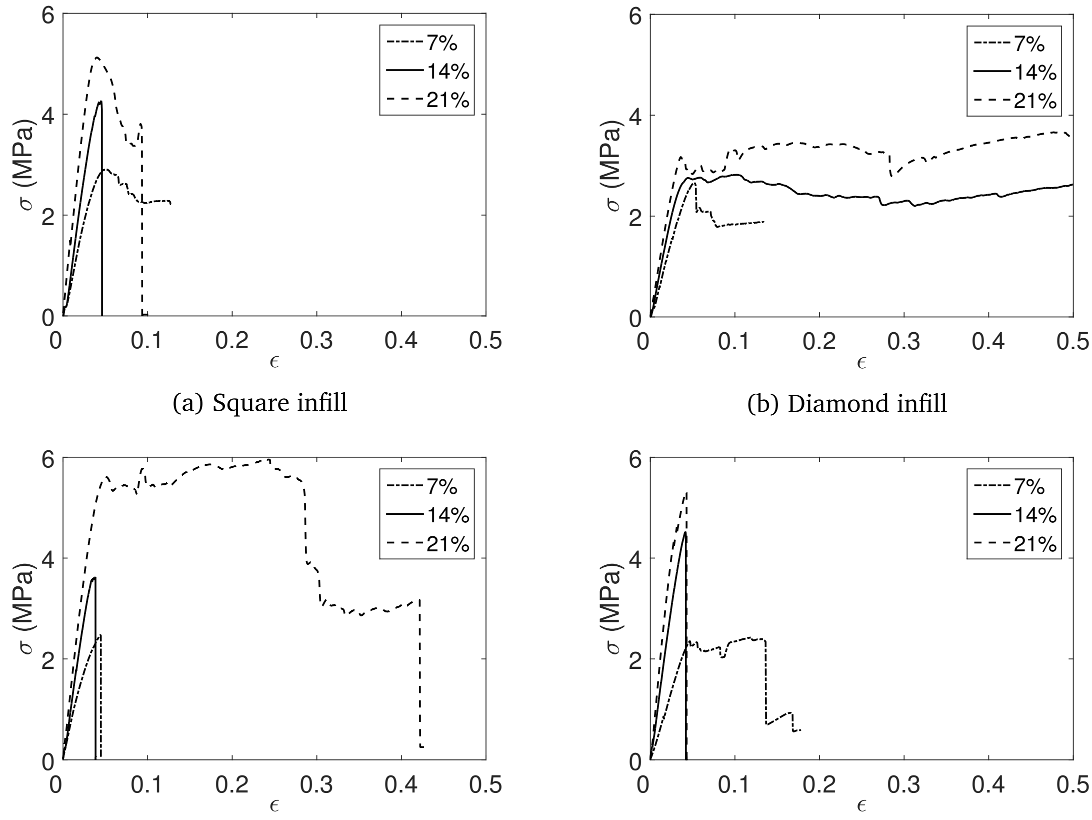

(a) Square infill

(b) Diamond infill

(c) 2D Honeycomb infill

(d) 3D Honeycomb infill

Figure 10: Stress-strain graphs for PLA tensile specimens

6.3 Discussion

The print quality of the lowest-density (7%) specimens was visibly poorer than that of the higher-density (14-21%) density prints. Quality problems arise due to insufficient adhesion between the liquid thermoplastic being extruded and the previously-deposited material on the printer bed. With high-density prints, there is a high surface area of material to which the newly-deposited thermoplastic can stick; with low-density prints, this surface area is lower, which can cause the extruded plastic not to remain where it was originally laid down. Insufficient adhesion leads to

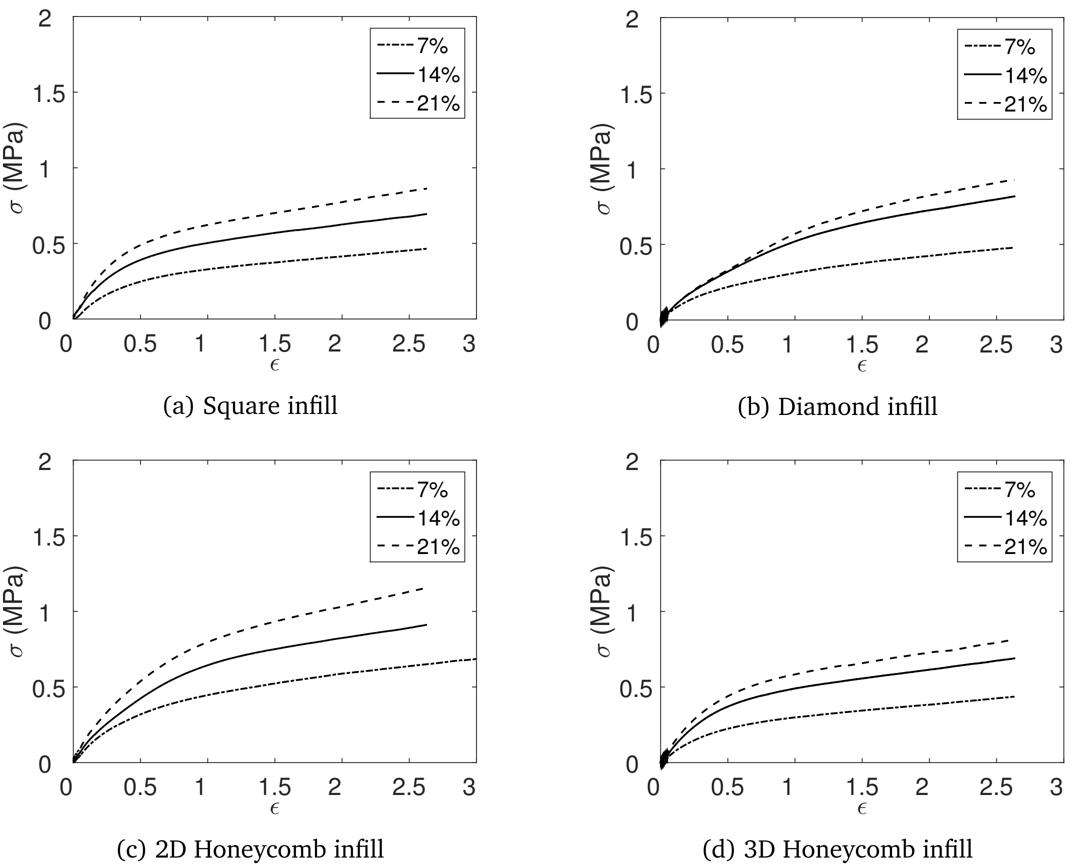

Figure 11: Stress-strain graphs for Ninjaflex tensile specimens

structural problems of two types: separation of consecutive, vertically-aligned layers (delamination), or separation of the infill from the perimeter.

Aside from the low reliability implied by poor print quality, another effect of the variability of structural integrity is that the low-density infills' strength was likely to have been over-estimated by the tensile tests. This is because the perimeter of the specimen continued to support load even after the infill structure had stopped doing so. This effect was proportionately more significant for the low-density structures, perhaps explaining why, for some infill patterns, there is a relatively small difference in the strength of structures of different infill density. For example, the 14% Square PLA structure had a yield stress only 2.6% greater than that of the 7% Square PLA structure.

It was also found that a small number of PLA specimens, such as those with 14% and 21% Diamond infill (Figure 10b), underwent much larger plastic strains before failure than other PLA specimens. This may be explained by the ductility of the material in the perimeter of the specimen, which was loaded in tension once the infill had failed. Despite these limitations, there is a clear correlation between infill density and both stiffness and strength. The relative performance of the infill patterns is less obvious, and requires further analysis.

7 Development

The information acquired about the studied materials and structures was used to conduct analysis on the multi-layered design chosen in Section 5.2.

The square frustum was split into $1 \leq n \leq 5$ layers of equal thickness. Moving from front to back, the layers have increasing average cross-sectional area, A_m. It was assumed that, during impact, the reaction force provided by the impact attenuator is uniform throughout the part. Dividing this force, $F_m = 60$kN, by A_m gives an average stress, σ_m, requirement for the structure of each layer. Columns 2-3 of Table 3 show the A_m and required σ_m values for all n assuming that the impact attenuator decelerates the car at the limiting average rate of $20g$.

n	A_m (mm^2)	σ_m (MPa)	Best Structure	ρ (kg/m^3)	m (kg)
1	62,500	0.96	42% Square	507.72	7.11
2	41,250	1.46	66% Square	793.80	8.50
	83,750	0.72	28% 2D Honeycomb	420.96	
3	34,167	1.76	56% Square	673.32	7.21
	62,500	0.96	42% Square	507.72	
	90,833	0.66	24% 2D Honeycomb	363.00	
4	30,625	1.96	92% Square	1,102.32	8.63
	51,875	1.16	50% Square	597.96	
	73,125	0.82	34% Square	402.12	
	94,375	0.64	24% 2D Honeycomb	363.00	
5	28,500	2.11	100% Square	1,200.00	8.91
	45,500	1.32	60% Square	710.88	
	62,500	0.96	42% Square	507.72	
	79,500	0.75	30% 2D Honeycomb	448.92	
	96,500	0.62	20% 2D Honeycomb	313.20	

Table 3: Values calculated in analysis of the multi-layer design

As discussed in Section 5.1, the key region of the stress-strain graph for energy absorption is that where, in foams, the stress plateaus with respect to strain, remaining approximately constant at a plateau stress, σ_p. PLA structures were rejected because, with the exception of the small number of abnormal cases discussed in Section 6.3, these exhibited brittle behaviour, with little or no stress plateau before failure. This implies that the energy absorbed, proportional to the energy density (area under the stress-strain curve), is low in these structures. For the Ninjaflex structures, the stress at 50% strain, $\sigma'_{0.5}$ was obtained by inspection of the stress-strain responses. This was used to approximate the average stress value during impact. An adjustment factor of 1.2 was applied to these stress values because, typically, plastics are roughly 20% stronger in compression than in tension [25]. The resultant stress is denoted by $\sigma'_{0.5}$.

In order to select the structure that fulfilled the functional requirement of each layer ($\sigma'_{0.5} = \sigma_m$) while minimising mass and cost, $\sigma'_{0.5}$ was plotted against the infill density. The structures tested did not have the full range of required $\sigma'_{0.5}$ given in Table 3. Therefore, a linear relationship between $\sigma'_{0.5}$ and infill density was assumed, and a first-order line of best fit was applied to the data points for each infill shape, allowing extrapolation for the estimation of $\sigma'_{0.5}$ for 0-100% infill density structures. Selection of the least dense functional structure for each layer comprised drawing a horizontal line at the required stress level, $\sigma'_{0.5} = \sigma_m$, and finding its intersections with the lines of best fit. The leftmost of these intersections corresponded to the infill pattern and density best suited to this layer.

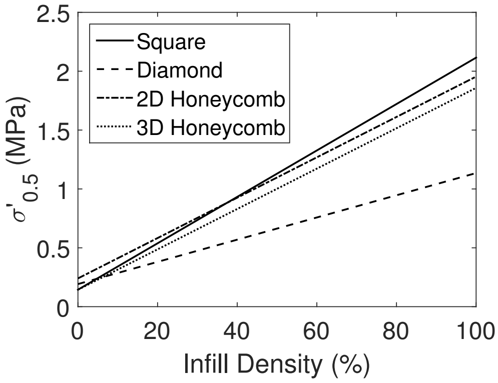

Figure 12: Plot used to identify suitable Ninjaflex infills in analysis of the multi-layer design

Table 3 shows the best structure for each layer, along with the resultant layer mass density, ρ, and total impact attenuator mass, m, for all n. ρ was found by using Slic3r to generate a 3D print file for a 100×100×100mm cube for the best structures identified for each layer. Contained in these print files is an estimate for the volume of material used in manufacture of the part. This was multiplied by the density of Ninjaflex, 1200kg/m^3, to give the mass of the cube [33]. Dividing by the cube's volume, 0.001m^3, gave ρ.

The results of this analysis suggest that a single-layer impact attenuator with a 42% Square Ninjaflex structure would be the lightest design. Because mass corresponds to the amount of material used in manufacture, this is also the design with the lowest cost. Therefore, this structure was selected for further analysis.

8 Finite Element Analysis

Abaqus finite element analysis (FEA) software [34] was used to compare the impact performance of the selected structure to a foam construction.

8.1 Validation

The results obtained from tensile testing were used to define a representative material in finite element (FE) models. The 21% Square Ninjaflex structure was used for a validation case to verify that the implementation of structure represented reality correctly. The material was defined as isotropic, with mass density, $\rho = 259$kg/m^3, Young's modulus, $E = 1.25$MPa, yield stress, $\sigma_y = 0.35$MPa, yield strain, $\epsilon_y = 0.28$, and plastic stress and strain values from the tensile testing results. Without results for transverse strain, Poisson's ratio, ν, had to be assumed to be the same as that of solid Ninjaflex, with a value of 0.4 [25].

A truncated version of the tensile specimen geometry, shown in Figure 13, was used to represent the fact that the specimen was gripped at both ends. One end face was constrained in all degrees of freedom; the other face was constrained in all degrees of freedom except for the direction of extension. The moving end face was displaced by 100mm in a general, static step. The default mesh settings – using 8-node, linear brick elements (of global length 3.2mm) with reduced in-

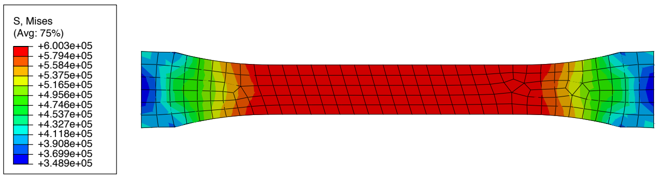

Figure 13: FE model used for the validation case (stress in Pa)

tegration and hourglass control – were used because the part geometry was simple. Maximum stress was plotted against maximum strain, which is shown in comparison to the same region of the graph from experimental testing of this structure in Figure 14.

The fact that these results have the same order of magnitude suggests that the structure has been implemented approximately correctly in the FE environment. The stress values returned by the numerical simulation are greater than the experimental values, possibly because the engineering stress normalisation used for the tensile testing results understimated the true stress.

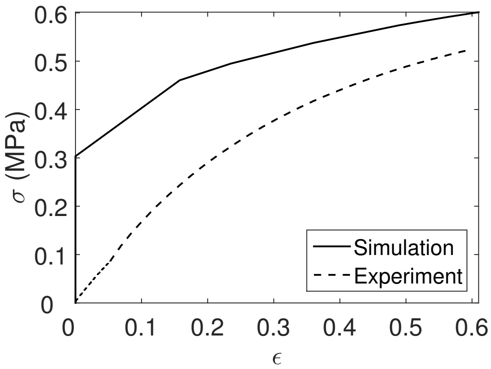

Figure 14: Comparison of results from numerical simulation and experimental testing

8.2 Impact Simulation

FE models of impact attenuators were made using the standard impact attenuator geometry and materials approximating the 42% Square Ninjaflex structure and the Rohacell 51WF foam used in a pre-existing design.

The impact attenuator was assembled between two rigid plates. The first of these, representing the unyielding wall, was constrained in all degrees of freedom, and was tied in contact with the front face of the impact attenuator. The second plate, representing the anti-intrusion plate, was constrained in all degrees of freedom except for the direction of impact velocity, and was tied in contact with the back face of the impact attenuator. The car was represented by a point mass of 300kg defined in the centre of the anti-intrusion plate. This point was assigned an initial velocity of 7ms^{-1}.

The stress and modulus values required to define the 42% Square Ninjaflex structure were found by applying a scale factor of 2 (assuming linear scaling of stress with infill density) to the experimental values obtained from tensile testing of the 21% Square Ninjaflex structure: $E = 2.28$MPa, $\sigma_y = 0.6$MPa, and the stress values in the plastic region. Strain and Poisson's ratio were unchanged from modelling of the 21% Square Ninjaflex structure: $\epsilon_y = 0.28$, $\nu = 0.4$. The density was taken from the Table 3: $\rho = 508\text{kg/m}^3$.

Implementation of the Rohacell foam followed the procedure used by Schormans (2010): the elastic region was defined by $E = 22.0\text{MPa}$, $\nu = 0$, $\sigma_y = 0.8\text{MPa}$ and $\epsilon_y = 0.05$; the plastic region used the crushable foam model with compression yield stress ratio, $k_t = 1.036$, hydrostatic yield stress ratio, $k = 0.1$, and stress-strain data from quasi-static testing; and the mass density, ρ was 52kg/m^3 [8]. k_t is the ratio of yield stress in uniaxial compression to yield stress in hydrostatic compression; k is the ratio of yield stress in hydrostatic tension to initial yield stress in hydrostatic compression.

The impact was simulated in a dynamic, explicit step with a duration of 50ms. As in the validation case, 8-node, linear brick elements were used because the part geometry was simple. A global element size of 10mm was used, which, in trial runs, produced the same results as with a finer mesh.

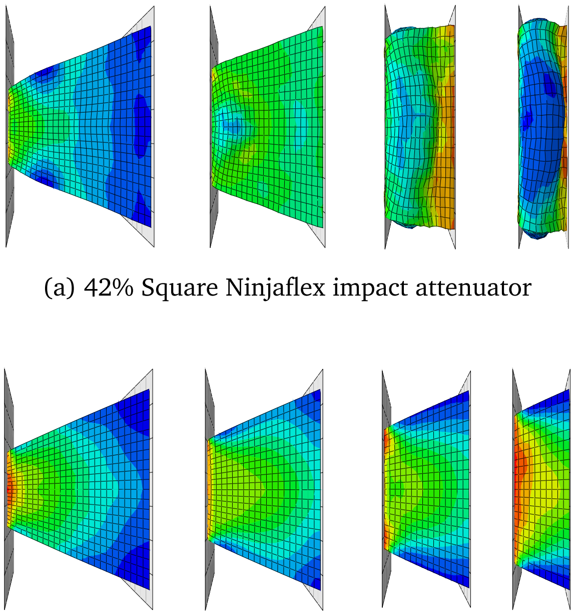

(a) 42% Square Ninjaflex impact attenuator

(b) Foam impact attenuator

Figure 15: Stress fields at multiple stages of impact simulation

Initial simulations encountered problems where, between time steps, the deformation wave initiated by impact travelled a distance greater than the length of the elements, causing the analysis to fail. This is common in FEA of impact loading on volumetrically-compacting materials, where deformations are large. It occurs because the strain gradients present in the model are too sharp for the mesh size. As advised by Abaqus documentation, to mitigate this effect, element distortion control was applied to the mesh. This function activates when elements exceed a threshold nominal strain, and has a dissipative effect on strain energy, reducing element distortion [35]. Relative to the kinetic energy of the system, the energy dissipated by the distortion control was small: a maximum of 134J in the Ninjaflex model, and less than 12J in the foam model.

Figure 15 shows the stress fields present in the parts at simulation times of 5ms, 12.5ms, 20ms and 35ms (left to right). These images illustrate the difference in how Ninjaflex and foam can be expected to deform under compression. Whereas the Ninjaflex part expands perpendicular to the direction of impact, the foam part crushes inwards, reducing its volume signifcantly.

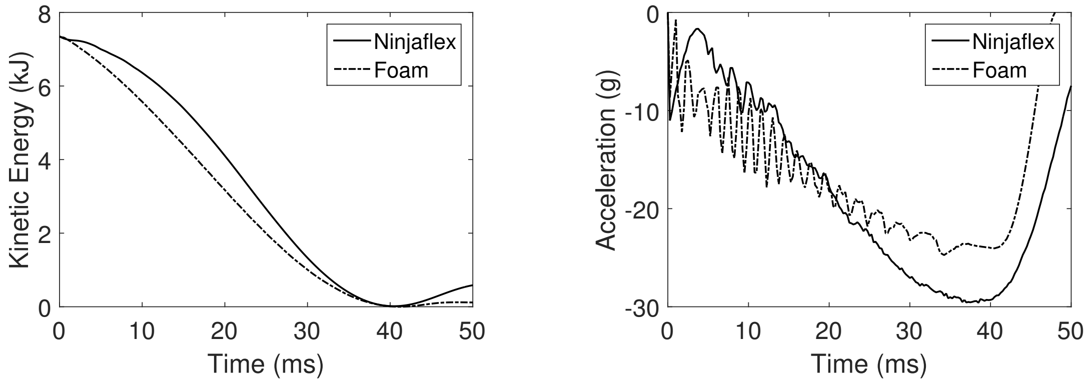

(a) Kinetic energy over time

(b) Acceleration over time

Figure 16: Impact simulation results

The results shown in Figure 16a suggest that the Ninjaflex structure performs similarly to the foam design, with both parts absorbing the car's impact energy in 40ms. Figure 16b shows that peak deceleration is approximately 20% greater with the Ninjaflex impact attenuator, however, suggesting that the driver would be more likely to be injured during the collision. Both impact attenuators lie within the allowed limit of mean deceleration: this was $30g$ for Ninjaflex, and $25g$ for foam.

8.3 Discussion

For a number of reasons, these simulation results should not be accepted as a proof of the Ninjaflex part's suitability. The assumption of isotropic behaviour of the Ninjaflex structure limits the validity of the model: extensive research has shown that the mechanical properties of 3D-printed parts are highly dependent on orientation [36]. Furthermore, Poisson's ratio had to be assumed to be the same of a solid material, which is unlikely given that the structure does not behave isotropically, as a solid does. These were necessary assumptions without enough information to define an anisotropic material in Abaqus, but the structure would not respond to load equally in all directions in reality.

Furthermore, strain rate effects are neglected. Tensile testing was carried out at relatively low strain rates compared to those involved in impact, so the stress-strain curves obtained experimentally will not reflect the equivalent curves obtained in high strain rate applications. Given that the experimental stress-strain curves were used to define the materials in the FE models, FEA predicted material behaviour as if loading were at the same rate as in tensile testing.

The use of element distortion control, which has a non-physical dissipative effect on the system's energy, implies reduced accuracy. However, the ability to quantify this effect revealed that, in relative terms, it was small (less than 2% of the system's maximum kinetic energy).

Due to these limitations, real-world tests were carried out to investigate the predictions of FEA.

9 Impact Testing

Impact testing on scale models was carried out to assess the performance of the final design in comparison to a pre-existing foam design.

9.1 Method

An Instron 9250HV drop weight test machine was used to test specimens made of Ninjaflex and foam. Due to the limited size of the machine's test bed, the outside dimensions of the impact attenuator were reduced by a length scale factor of 0.2. Ninjaflex specimens were printed in two orientations on the 3D printer bed, resulting in different infill orientations, as depicted in Figure 17. No skin layer was applied to the outside of the infill.

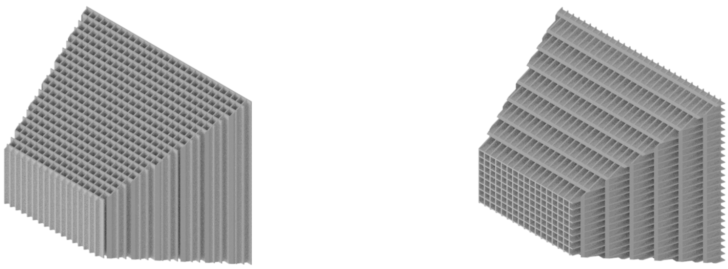

(a) Printed upright (b) Printed with back face on bed

Figure 17: Infill orientations used for 3D-printed impact test specimens

The foam specimens used the three-layer construction previously used by Foster (2015), making use of foam with decreasing density from front to back. The front layer was made of Rohacell 71IG-F, the middle of Rohacell 51IG-F, and the back layer of Rohacell 31IG-F. These layers were cut to the correct size and shape using a band saw, then bonded together with wood glue [9].

The specimens were placed on a 3mm-thick plate of aluminium to reflect mounting on an anti-intrusion plate on the car. In order to prevent the specimens from moving, trapezoidal blocks of plywood were placed either side of the specimens and clamped to the testing platform with G-clamps, as shown in Figure 18. A 50mm-diameter, 50mm-length aluminium roller impacter was used because its frontal area approximately matched the average cross-sectional area of the specimens. The total mass of the impacter assembly was 7.5kg.

A review of the use of scale models in impact tests found no clear relationship between length scale factor and energy absorption scale factor. Therefore, energy absorption was assumed to scale linearly with volume (or the cube of length); impact energy was set to $7350 \times 0.2^3 = 58.8$J, achieved by releasing the impacter from a height of 0.8m above the specimen's top face.

The impacter was attached to a 10kN load cell, which measured the reaction force provided by the specimen. This force data, along with values for displacement, was output at a frequency of 0.5MHz. The output data contained significant noise, so the `smooth` MATLAB function was used, applying a moving average filter at an interval of 800 data points (see Appendix B). The work done by the impacter on the specimen was found by finding the area under the force-displacement graph. Kinetic energy was calculated by subtracting the work done from the impact kinetic energy, 58.8J. The acceleration of the impacter was found by dividing the reaction force by the impacter assembly's mass of 7.5kg. Kinetic energy and acceleration were plotted against

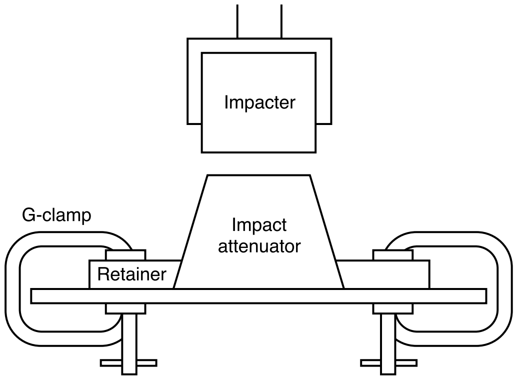

Figure 18: Impact test apparatus

time, as shown in Figure 19.

In order to avoid potential damage to the load cell by exceeding its rated load, the stroke of the impacter could not be set to extend through the whole length of the specimens. Instead, the impacter was permitted to pass approximately 45mm below the top face of the specimens, after which pneumatic pistons activated, decelerating the impacter assembly. This limited the impact duration to approximately 15ms.

A repeat test was carried out for each specimen type to ensure that anomalous results were not used for comparison. In order to analyse the deformation of the specimens under impact, a Photron SA1 high-speed camera was used to video the specimens during impact at a rate of 10,000 frames per second.

9.2 Results

Figure 19 shows a comparison of the impact responses of the three types of specimen, where ‘Ninjaflex A’ refers to the orientation depicted in Figure 17a, and ‘Ninjaflex B’ refers to the orientation depicted in Figure 17b.

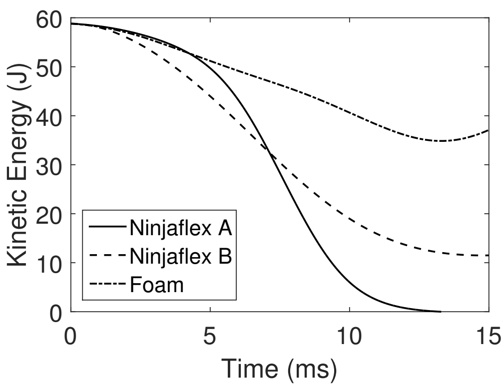

(a) Kinetic energy over time

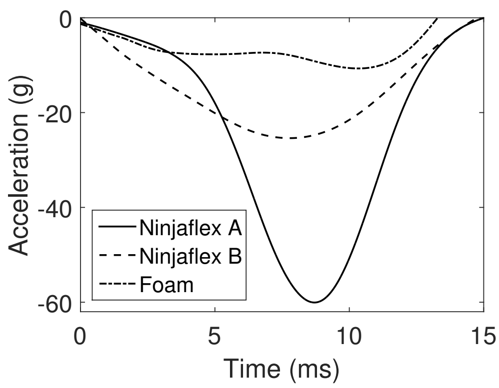

(b) Acceleration over time

Figure 19: Impact test results

The only specimen type to absorb all of the impacter’s kinetic energy before the pneumatic pistons were activated was Ninjaflex A. The Ninjaflex B specimen absorbed roughly 80% of the impact energy, while the foam specimen absorbed less than 50%. Appendix B contains a summary of the mean deceleration, a_m, peak deceleration, a_p, and kinetic energy at 15ms, e_k, for the tests of two specimens of each type. The Ninjaflex A specimen decelerated the impacter at a rate greater than permitted by the Formula Student rules, while the other specimen types lay within the limits set by the regulations.

9.3 Discussion

The foam specimens demonstrated a low rate of energy absorption, hence the high value of impacter kinetic energy even after 15ms. Inspection of the videos of impact revealed that, due to the difference in the density and stiffness of each layer, the layers crushed sequentially, starting from the least dense layer at the bottom (see Figure 20). Because the impacter stroke was not long enough for the top layer to be crushed, no work was done to compress this layer, leaving levels of kinetic energy high. This reveals the limitations of testing without the ability to destroy the specimen: if the full length of the foam part were used, it might have absorbed all of the impact energy.

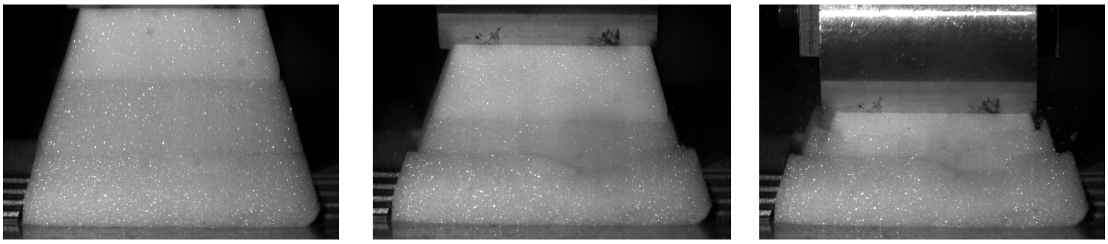

(a) Before crushing (b) Bottom layer crushed (c) Middle layer crushed

Figure 20: Sequential crushing of foam specimen layers

In contrast, the Ninjaflex A specimens absorbed kinetic energy quickly, but this came at the expense of safe rates of deceleration. This suggests that the 42% Square Ninjaflex structure is too stiff in this orientation. Through inspection of the videos of impact, it was found that this excessive stiffness resulted in the anti-intrusion plate bending as the impacter reached the end of its stroke. All Ninjaflex specimens exhibited elastic behaviour, returning to their original shape and size after impact. This suggests that kinetic energy was transduced not by plastically deforming the constituent material but rather by deforming sections of the infill macro-structure in tension, compression or bending, storing elastic potential energy.

The Ninjaflex B specimens represented a compromise between the foam and Ninjaflex A, dissipating most of the impacter's kinetic energy in 15ms while decelerating it at a rate permitted by the rules. The significant difference between the performance of Ninjaflex A and B underlines the anistropy of 3D-printed parts.

While these results are useful for evaluation of the designs relative to each other, it cannot be assumed that a full-scale impact attenuator with the same construction would absorb a linearly-scaled amount of kinetic energy, or do so at the same rate of deceleration as provided by these specimens. Extensive work has found that geometrically-similar scaling does not tend to be valid for mechanical properties. For example, typically, scale models over-estimate the strength of the full-scale part. Jones (1996) brings together results from multiple experiments on energy absorption in scale models, all of which suggest that the energy absorption scale factor lies in between the cubic (volume) law and the square (area) law. This means that energy absorbed by the full-scale model could be less than 50% of the expected value [37].

With information about the tested structures' strain rate sensitivity, FEA could be used to find an empirical relationship between length scale and energy absorption. However, this information was not known for Ninjaflex structures used.

10 Discussion

Recommendations are made based on the performance of the final design relative to foam alternatives. The choice of design constraints and variables is discussed. Findings on the subject of 3D printing are summarised, after which suggestions are made for areas of future work.

10.1 Final Design

Both simulated and real-world impact tests allowed the 42% Square Ninjaflex structure to be compared to a polymer foam in terms of performance. FEA predicted that Ninjaflex would behave similarly to foam, fulfilling the functional requirement of absorbing 7350J of energy without decelerating the car at an average rate greater than $20g$ or a peak rate greater than $40g$. Real-world testing revealed that the infill orientation of the Ninjaflex part determined whether or not it fulfilled the functional requirements: Ninjaflex A specimens did not function, but Ninjaflex B specimens did. Compared to the foam design, both types of 3D-printed structure decelerated the moving body at a greater rate than achieved by the foam.

In addition to poorer impact performance compared to the foam equivalent, the Ninjaflex impact attenuators were almost 10 times heavier than the same part made of Rohacell 51WF. The material cost of printing the full-size impact attenuator with 42% Square Ninjaflex infill would be approximately £520 [19]. The Rohacell foam used in Bristol Electric Racing's 2014-15 impact attenuator design was procured in the form of offcuts, incurring zero cost. Therefore, in this form, the 3D-printed impact attenuator does not offer any progress towards the design objectives of mass and cost minimisation.

The notable implication of the Ninjaflex part's anisotropic behaviour is that it cannot be assumed to perform well in off-axis impacts, where the direction of the reaction force may have profound effects on the structure's response. Therefore, the use of Ninjaflex instead of foam, which is roughly isotropic [23], for the impact attenuator would imply a compromise on the grounds of reliability.

Therefore, use of the final 3D-printed impact attenuator is not recommended: it causes greater rates of deceleration than the foam equivalent; its level of reliability in off-axis impacts is unknown; it weighs more than the foam part; and manufacture would be costly.

10.2 Part Selection

It could be argued that pursuit of mass reduction with a part already weighing less than 1kg – in the context of a Formula Student car weighing approximately 300kg – should not be of high priority. Indeed, foam is highly specialised for energy absorption with low mass density, so a significant improvement may be difficult to find.

10.3 Design Specification & Process

Constraining the project to the use of the Replicator 2 with PLA and Ninjaflex significantly limited freedom when selecting a mechanism for dissipation of kinetic energy. The ability to print metallic parts would permit the investigation of alternatives to the crushing mechanism investigated, such as buckling mechanisms employing plastic hinges. The use of a higher-resolution printer would enable the the manufacture of more sophisticated internal structures than those studied. These may take a form similar to the microlattice structure created by a team at HRL Laboratories (2011). This structure is comprised of interconnected hollow metal tubes with 100 nanometre wall thickness, and is both lightweight and energy-absorbent [39].

Although removal of these constraints would have resulted in a greater scope of research, it was possible to arrive at a functional final design while observing these constraints. Therefore, they were not so restrictive that no solution could be found. Furthermore, the fact that the final design, albeit limited, was functional, suggests that the analysis of the multi-layer design in Section 7 was sound. This is partly because the use of the parallel multi-layer design permitted clear like-for-like comparison of 3D-printed infills to foams. Using this previously-used macro-structure for the new design allowed deduction that any difference in the behaviour of the designs is solely due to the effective mechanical properties of each layer. Thus, the choice of multi-layer construction type clarified analysis and development.

One of the key variables in the study was the infill pattern. It is evident from Figure 12 that there was little difference between the stress-strain responses of the patterns tested. This was unexpected, but could be explained by the inclusion of a perimeter when printing the specimens. This strengthened all of the specimens, masking the potentially-subtle effects of infill cell shape. Tests on specimens with no perimeter would have made the relationship between pattern and stress-strain response clearer. Given that Figure 12 consists mainly of extrapolated values, this may not reflect the true difference between patterns. Investigation of a greater range of infill densities would, therefore, also clarify the difference between patterns.

To summarise, the choice of constraints necessarily limited the scope of research and innovation. The selection of the parallel multi-layer design made analysis, development and comparison to the pre-existing design more straightforward than would be the case if a new macro-structure were used. The effect of changing the design variables used was less clear and smaller than expected, but the results obtained were instructive enough to develop a working impact attenuator design.

10.4 3D Printing

A key finding was the extent to which low infill density 3D-printed parts are susceptible to poor print quality. To varying degrees, almost all specimens made with less than 10% infill exhibited defects. This problem was rare in parts with higher infill density.

Experimenting with slicing software revealed that the package used to convert design files to 3D print files seemed to have a noticeable effect on adhesion between deposited layers. Makerbot Desktop, the default software for use with the Replicator 2, was found to produce higher-quality prints than Slic3r – the package used for this research – at lower infill densities. This may be explained by differences in the algorithms used to generate infill patterns. Therefore, although it was thought that Slic3r was the better option because it offered a greater degree of control over print settings, using Makerbot Desktop may have resulted in higher-quality prints.

Due to the variation in print quality depending on infill, it is expected that 3D-printed parts do not have a universal level of reliability; confidence in the part's performance is linked to the settings used in printing. Therefore, for applications where failure could have dangerous or costly consequences, extensive testing of samples is recommended.

Aside from the quality issues associated with 3D printing using the Replicator 2, there are further caveats to consider when using this manufacturing process. Firstly, for simple geometries, the time taken to 3D print part is long relative to how long it would take to make the same part with traditional techniques. For example, cutting the foam into the shape of the impact test specimens took less than 5 minutes per part, while printing the specimen with the infill orientation shown in Figure 17a took over 5 hours. The slow manufacture speed is acceptable when the complexity of a part's geometry makes traditional manufacture either impossible or similarly slow. However, for shapes such as the square frustum studied, 3D printing may not be necessary if there exist solid materials with the desired material properties (foam in this case). Indeed, the final design did not fully take advantage of the unique capabilities of 3D printers, instead effectively attempting – and failing – to replicate a homogeneous, isotropic material.

A second caveat is the cost of 3D printing. Even if the sunk cost of the initial purchase of the 3D printer is ignored, the print cost is significant for large parts made with high infill density, purely on the basis of material cost. As with the speed of manufacture, this should not deter the use of 3D printing for the majority of applications, but it is less likely to be a cost-effective manufacturing technique for large objects. One way of reducing the average cost of prints would be to recycle the material in parts that either print poorly, break in use or are no longer needed. One method of doing this is to use a machine to grind up parts into small pellets, which can be melted and formed into an extrusion [38]. Indeed, a significant advantage of using thermoplastics is the potential to reuse waste material.

10.5 Experimental Approach

It was initially thought that a purely empirical, iterative approach, where designs would be impact tested then developed before further testing, could be used. However, it was decided that the results of impact testing would not provide sufficient meaningful information to direct the adjustment of designs. This is why quasi-static testing was used to characterise the 3D-printed structures of interest, allowing for informed analysis.

The decision to select tensile testing instead of compressive testing was made with the assumption that the transverse strain of the tensile specimens could be measured, enabling the calculation of effective Poisson's ratio for the structures. However, the video extensometers required for measuring this strain were unavailable at the time of testing. Tensile testing also permitted the application of strains greater than 100%, resulting in the extended stress-strain graphs shown in Figure 11, but these levels of strain are not applicable to compressive applications. Therefore, the rationale for selecting tensile testing was perhaps not sound.

In retrospect, compressive testing of cuboidal specimens may have been a better choice of testing method. The structures' response to compressive loading would more accurately reflect the behaviour of the infills under impact loading, making the approximate adjustment factor used in Section 7 unnecessary. Using cuboidal specimens with a greater cross-sectional area than that of the tensile specimens would have an averaging effect, spreading the load over a greater number of infill pattern cells. This would reduce the likelihood of a localised print error having a significant effect on the recorded strength of the specimen. Therefore, by using tensile testing, the quality of results obtained was perhaps not as high as it could have been.

The experimental approach generated information about the effect of changes in material, infill pattern and infill density on the macro-scale behaviour of structures. The advantage of this macro-scale work is that it avoids the oversimplifications often implied by purely theoretical modelling, and generally takes systematic effects – those that apply to all structures – into account. The disadvantage of this approach is that the mechanics of failure are not fully understood, so design progression is partly guided by intuition.

The use of FEA to test the infill structure chosen in Section 7 was valuable to predict performance relative to foam. Given that previous work had confirmed the suitability of foam for construction of impact attenuators, a sense of how the 3D-printed part might perform in reality was gained. However, the limitations of the FE model prevented any further conclusions from being drawn without real-world impact testing results.

The impact testing method also had drawbacks – notably, the inability to destroy the specimen fully without risking damage to the load cell. However, the information obtained was sufficient to reject one design, Ninjaflex A, while comparing the other two, Ninjaflex B and foam. If the Ninjaflex B design had had a reduced mass or cost compared to the foam design, it would have been valuable to conduct off-axis impact tests on it. Given that neither of these was true, these further tests were surplus to requirements in order to make a recommendation.

10.6 Future Work

It should be considered that, because a functional foam impact attenuator can weigh less than 1kg, any mass reduction achieved by simply redesigning this part will have a proportionately small effect on the total mass of the car. However, there is scope for more significant mass reduction by combining previously-separate components into a single part. In the case of the impact attenuator, this would involve including its energy absorbing function into the design specification of the nose cone. Manufacture of the new nose cone could be achieved with traditional techniques and materials, such as CFRP – a material whose suitability for this application was discussed in Section 3.

If further research into 3D printing energy-absorbent structures is chosen, the investigation of alternative materials to PLA and Ninjaflex is recommended. During the analysis performed in Section 7, it became evident that it would be desirable to find a compromise between the properties of the Ninjaflex and PLA structures tested, with the former exhibiting a relatively flat stress-strain response, and the latter offering higher strength. This compromise may be offered by a stiffer, stronger form of thermoplastic polyurethane, Semiflex, from the same manufacturer as Ninjaflex [40]. With a stronger base material, it might be possible to use structures with lower infill densities, reducing the mass of the part. Therefore, research into energy absorption of Semiflex infills is recommended. If FEA is chosen as a stage of development towards a final design, the FE model should be defined in a way that reflects the anistropic nature of parts made by the FDM 3D printing technique.

Research could be carried out on the use of high-resolution laser sintering machines to produce metallic 3D-printed parts with intricate, thin-walled internal structures. It should be noted that specific energy absorption should not be used as the only parameter investigated for application to the impact attenuator; the value of plateau stress is also important because it determines the rate at which the car is decelerated, affecting safety.

Finally, the principle of topology optimisation – where strategic placement of material is used to satisfy functional requirements while maximising the extent to which objectives can be achieved – could be applied to design of the impact attenuator through the use of software such as Altair Hyperworks [41].

11 Conclusions

Given the manufacturing and material constraints applied to the project, the impact attenuator was a suitable selection as the car part for study. This is shown by the fact that a 3D-printed design was able to be developed, manufactured and proven to function, in limited scenarios, using numerical simulations and experimental testing. The development process had limitations: the use of tensile testing to characterise 3D printed structures; the inaccuracy of the FE models used for impact simulations; and the requirement to use scale models for final, real-world impact testing. However, the results obtained were sufficient to make a comparison between the new design and a pre-existing one. This revealed that the 3D-printed impact attenuator offers no meaningful improvement over the pre-existing foam part: it neither performed as well as the foam part, nor reduced mass, nor reduced cost. Despite this, the research was valuable for the insight it gave into using 3D printing as a manufacturing process for end products rather than just for prototypes. This informed recommendations for future work in the areas of energy absorption and 3D printing for Formula Student.

References

[1] Institution of Mechanical Engineers (2016) *Formula Student*. Available from `formulastudent.imeche.org/formula-student` [Accessed 28 March 2016].

[2] Ford, M. (2015) *The Rise of the Robots: Technology and the Threat of Mass Unemployment*. Oneworld Publications.

[3] 3T RPD (2016) *Automotive Case Studies*. Available from `3trpd.co.uk/case-studies` [Accessed 31 March 2016].

[4] Makerbot (2012) *Makerbot Replicator 2 Desktop 3D Printer Sets New Standard in Desktop 3D Printing*. Available from `makerbot.com/replicator2-press-assets` [Accessed 31 March 2016].

[5] SAE International (2014) *2015 Formula SAE Rules*.

[6] The Dow Chemical Company (2015) *Product Safety Assessment: IMPAXX Energy Absorbing Foam*.

[7] BSCI Energy Impact Systems (2016) *Impact Attenuator*. Available from `rollbarpadding.com/product/id-48` [Accessed 3 April 2016].

[8] Schormans, J. (2010) *The Design of a Formula Student Front Impact Attenuator*. Eindhoven University of Technology.

[9] Foster, G. (2015) *The Design and Manufacture of an Impact Attenuator for a Formula Student Car*. University of Bristol.

[10] Boria, S. (2010) Behaviour of an Impact Attenuator for Formula SAE Car Under Dynamic Loading. *International Journal of Vehicle Structures & Systems*, 2.

[11] Hart, J., Kennedy, C., LeClerc, T. & Pollard, J. (2010) *FSAE Impact Attenuator*. Worcester Polytechnic Institute.

[12] Oshinibosi, A. (2012) *Chassis and Impact Attenuator Design for Formula Student Race Car*. University of Leeds.

[13] Munusamy, R. & Barton, D. (2010) Lightweight Impact Crash Attenuators for a Small Formula SAE Race Car. *International Journal of Crashworthiness*, 15.

[14] Wang, J., Zhao, J., Liu, T., He, Z., Li, K. & Yang, W. (2015) Crash Analysis of Composite Energy-Absorbing Cylindrical Impact Attenuator. *Journal of Reinforced Plastics & Composites*, 34.

[15] Boria, S. & Belingardi, G. (2014) Composite Impact Attenuator with Shell and Solid Modelling. *11th World Congress on Computational Mechanics*.

[16] Boria, S. & Pettinari, S. (2014) Mathematical Design of Electric Vehicle Impact Attenuators: Metallic vs Composite Material. *Composite Structures*, 115.

[17] Yang, Y., Wu, X., Terada, S., Okano, M., Nakai, A. & Hamada, H. (2012) Application of FRP in a Vehicle for Student Formula SAE Competition of Japan. *International Journal of Crashworthiness*, 17.

[18] Makerbot (2016) *Makerbot PLA Filament*. Available from `store.makerbot.com/filament/pla` [Accessed 3 April 2016].

[19] NinjaTek (2016) *Ninjaflex Flexible 3D Printing Filament by NinjaTek*. Available from `fennerdrives.com/product-lines/_/3d/?=` [Accessed 18 April 2016].

[20] Ashby, M. & Jones, D. (2005) *Engineering Materials 1: An Introduction to Properties, Applications and Design*, Third Edition. Elsevier Butterworth-Heinemann.

[21] Shigley, J. & Uicker, J. (1980) *Theory of Machines and Mechanisms*. McGraw-Hill.

[22] Qiao, P., Yang, M. & Bobaru, F. (2008) Impact Mechanics and High-Energy Absorbing Materials: Review. *Journal of Aerospace Engineering*, 21.

[23] Gibson, L. & Ashby, M. (1999) *Cellular Solids: Structure and Properties*, Second Edition. Cambridge University Press.

[24] Hammetter, C., Rinaldi, R. & Zok, F. (2013) Pyramidal Lattice Structures for High Strength and Energy Absorption. *Journal of Applied Mechanics*, 80.

[25] Granta Design Limited (2015) *CES EduPack 2015*.

[26] BMW Team (2008) Materials in the BMW Sauber Formula One Race Car. *Advanced Materials & Processes*, 166.

[27] Makerbot (2016) *Makerbot Desktop*. Available from `makerbot.com/desktop` [Accessed 10 April 2016].

[28] Alessandro Ranellucci (2016) *Slic3r*. Available from `slic3r.org` [Accessed 10 April 2016].

[29] ASTM International (2014) D638. *Standard Test Method for Tensile Properties of Plastics*. ASTM.

[30] Al-Maliky, N. (1997) *Strain Rate Behaviour of Thermoplastic Polymers*. Loughborough University.

[31] National Physical Laboratory (2007) *Manual for the Calculation of Elastic-Plastic Materials Models Parameters*. Queen's Printer for Scotland.

[32] Mathworks (2016) *MATLAB 2016a*.

[33] Fenner Drives (2014) *Ninjaflex Safety Data Sheet*.

[34] Dassault Systèmes (2014) *Abaqus/CAE 6.14*.

[35] Abaqus Inc. (2005) Lecture 2: Elements. *Abaqus/Explicit: Advanced Topics*.

[36] Ahn, S.-H., Montero, M., Odell, D., Roundy, S. & Wright, P. (2002) Anisotropic Material Properties of Fused Deposition Modelling ABS. *Rapid Prototyping Journal*, 8.

[37] Jones, N. (1996) Some Comments on the Scaling of Inelatic Structures Loaded Dynamically. *Size-Scale Effects in the Failure Mechanisms of Materials and Structures*. Chapman & Hall.

[38] Dennon Oosterman (2014) *ProtoCycler: Free, Sustainable 3D Printer Filament*. Available from `indiegogo.com/projects/protocycler-free-sustainable-3d-printer-filament#/` [Accessed 18 April 2016].

[39] Schaedler, T., Jacobsen, A., Torrents, A., Sorensen, A., Lian, J., Greer, J., Valdevit, L. & Carter, W. (2011) Ultralight Metallic Microlattices. *Science*, 334.

[40] NinjaTek (2016) *Semiflex 3D Printing Filament*. Available from `ninjaflex3d.com/products/semiflex/` [Accessed 18 April 2016].

[41] Altair Engineering (2016) *Hyperworks*. Available from `altairhyperworks.co.uk` [Accessed 19 April 2016].

A Tensile Testing

The following MATLAB script was used to process the tensile testing data:

```
%Retrieve data from spreadsheet
data = csvread('test.csv',2,1);
force = data(:,2);
extension = data(:,1);

%Normalise force and extension
stress = force./41.6;
strain = extension./57;

%Plot stress-strain curve
l = plot(strain,stress,'color','black', ...
'linewidth',1.5,'linestyle','-');

%Accounting for noise: take sample of stress and strain
%every 200 data points
stress_sample = stress(1:200:end);
strain_sample = strain(1:200:end);

%Find gradient at each sampled point
E = gradient(stress_sample,strain_sample);

%Find stress and strain at point where gradient falls
%below 95% of its original value
yield_stress = stress_sample(find(E/E(1)<0.95,1));
yield_strain = strain_sample(find(E/E(1)<0.95,1));

%Find average gradient in elastic region
E_mean = yield_stress/yield_strain;

%Find y-intersect of line passing through 0.2% strain with
%gradient E_mean
offset_y_intersect = -1*(0.002./E_mean);

%Find strain range in which to plot elastic region line of best fit
max_stress = 10;
offset_max_strain = max_stress/E_mean;
offset_strain_range = 0.002:0.002:offset_max_strain;

%Evaluate line of best fit
offset_line = polyval([E_mean offset_y_intersect], ...
offset_strain_range);

%Find intersection between stress-strain curve and line of best fit,
%defining offset yield point and re-evaluating average modulus
[x,y] = polyxpoly(strain,stress,offset_strain_range,offset_line);
yield_stress = y;
```

```
yield_strain = x;
E_mean = yield_stress/yield_strain;

%Format figure
axis([0 0.5 0 6])
set(gcf,'color','white')
set(gca,'xtick',0:0.1:0.5)
set(gca,'ytick',0:2:6)
set(gca,'xticklabel',0:0.1:0.5)
set(gca,'yticklabel',0:2:6)
set(gca,'fontsize',20)
xlabel('\epsilon')
ylabel('\sigma (MPa)')
```

Table A1 shows the results selected for plotting in Figures 10 and 11. Figures A1 and A2 show all of the tensile results obtained for PLA and Ninjaflex respectively. The colour of the line plotted indicates the test number for the given specimen type: black for test 1; red for test 2; blue for test 3; green for test 4; and magenta for test 5.

Material	**Pattern**	**Density (%)**	σ_y **(MPa)**	ϵ_y	E' **(MPa)**
PLA	Square	7	2.49	0.04	70.88
		14	4.16	0.04	101.71
		21	4.20	0.02	178.46
	Diamond	7	2.34	0.04	57.21
		14	2.40	0.03	77.77
		21	2.80	0.03	98.59
	2D Honeycomb	7	0.93	0.01	79.44
		14	3.22	0.03	110.11
		21	4.40	0.03	146.29
	3D Honeycomb	7	2.17	0.04	53.11
		14	4.07	0.04	116.01
		21	4.20	0.03	163.07
Ninjaflex	Square	7	0.16	0.24	0.65
		14	0.25	0.23	1.09
		21	0.35	0.28	1.25
	Diamond	7	0.02	0.02	0.81
		14	0.14	0.17	0.85
		21	0.21	0.26	0.79
	2D Honeycomb	7	0.20	0.24	0.84
		14	0.25	0.23	1.05
		21	0.35	0.28	1.25
	3D Honeycomb	7	0.12	0.19	0.63
		14	0.33	0.41	0.81
		21	0.16	0.12	1.31

Table A1: Selected tensile test results for each specimen type

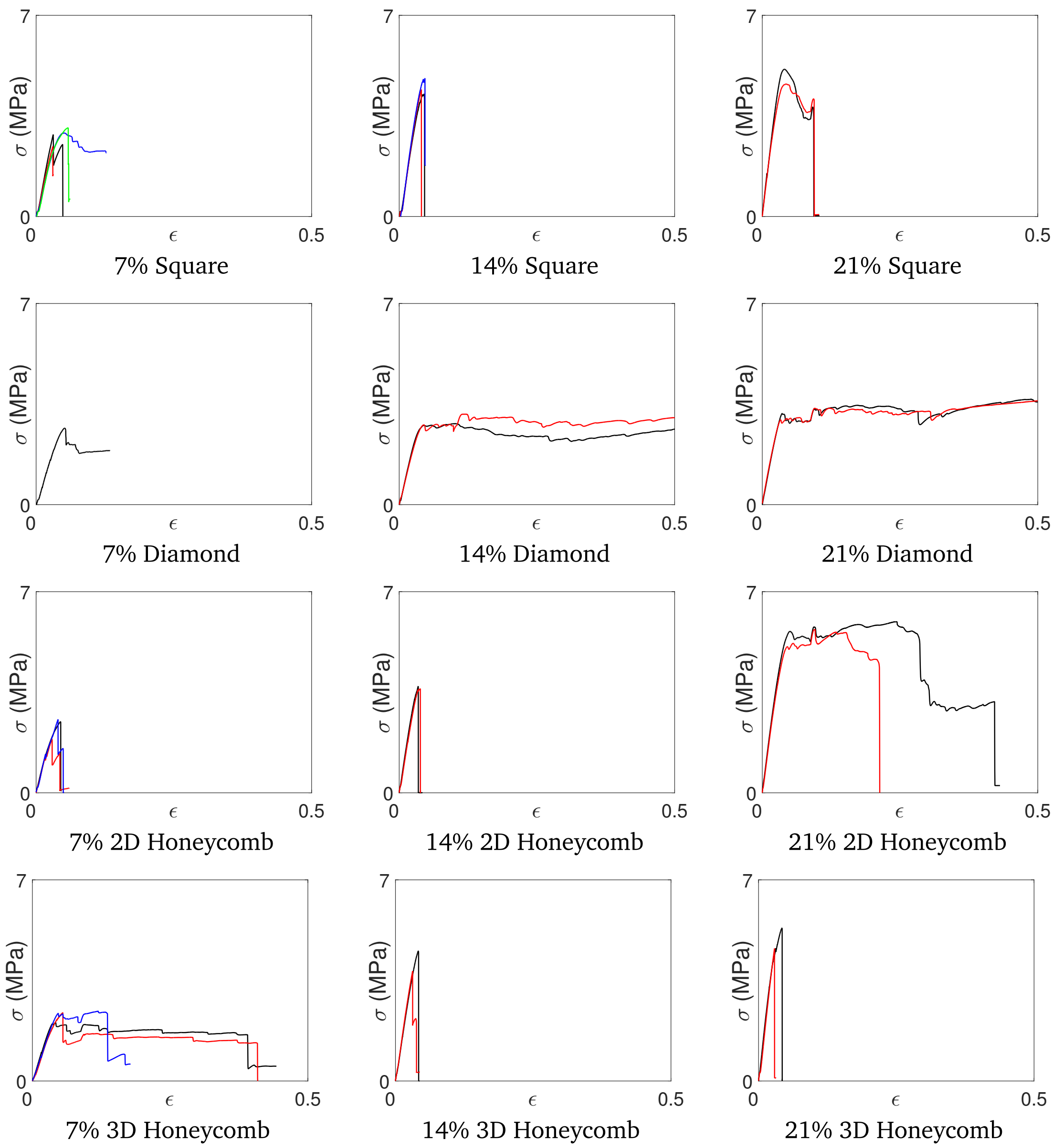

Figure A1: Plots of all tensile stress-strain data for PLA

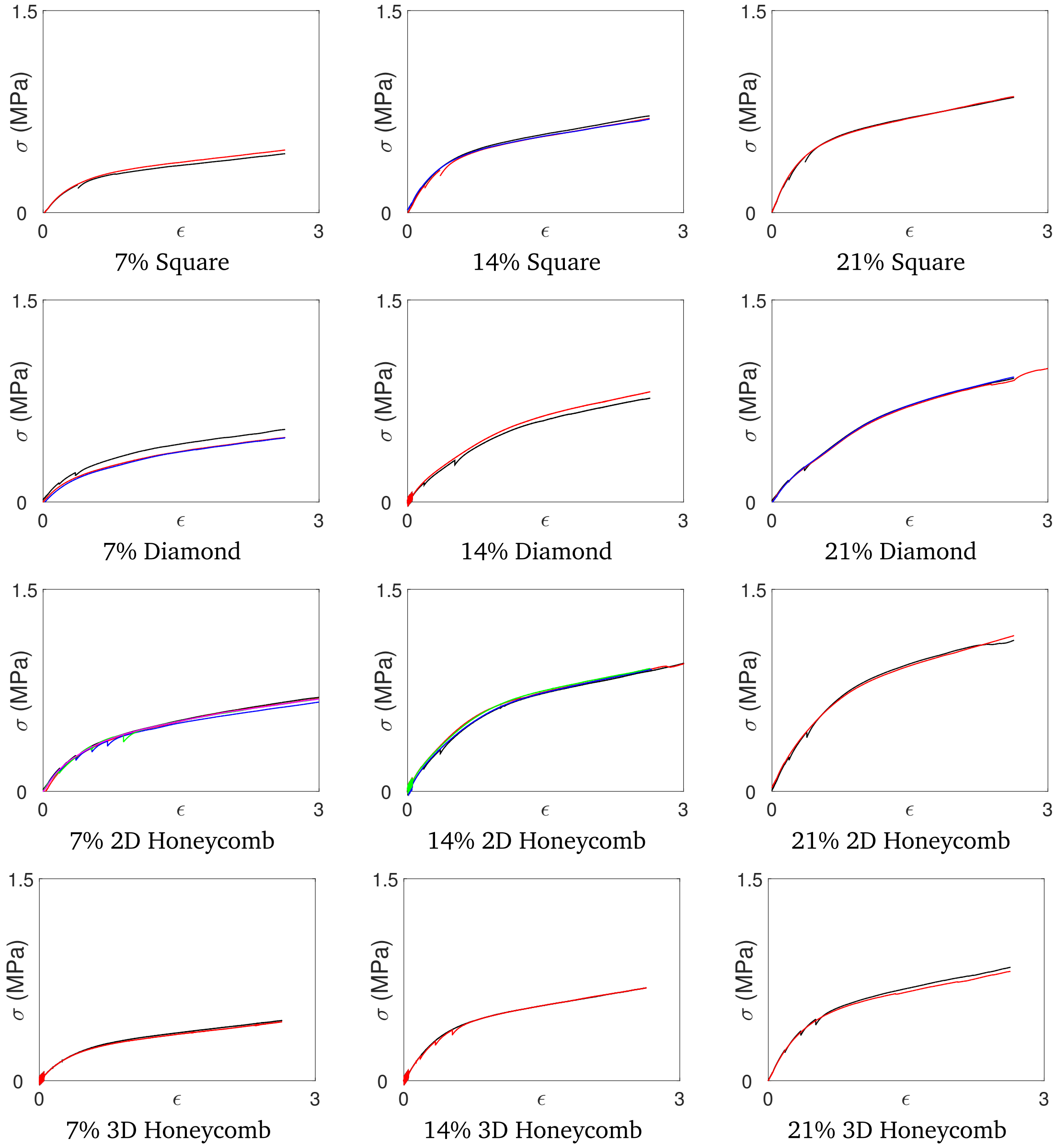

Figure A2: Plots of all tensile stress-strain data for Ninjaflex

B Impact Testing

The following MATLAB script was used to process impact testing data:

```
%Retrieve data from spreadsheet
file = strcat('test',test,'b.csv');
data = csvread('test.csv',8,0);
time = data(:,2);
load = data(:,4);
deflection = data(:,7);
```

```
%Accounting for noise: apply a moving average filter
load = smooth(load,800,'lowess') .* 1000;
acc = load ./ (7.5*9.81*-1);

%Look at time before pneumatic pistons activate
impact_time = time(find(time<15);
impact_load = load(find(time<15));
impact_deflection = deflection(find(time<15);
impact_acc = acc(find(time<15);

%Find cumulative work done and subtract from
%impact energy to give kinetic energy
cum_work = cumtrapz(impact_deflection,impact_load);
ke = 58.8 - cum_work;

%Find acceleration values
mean_acc = mean(impact_acc);
peak_acc = min(impact_acc);
```

Figure B1 shows the effect of the smoothing function used on the impact testing data.

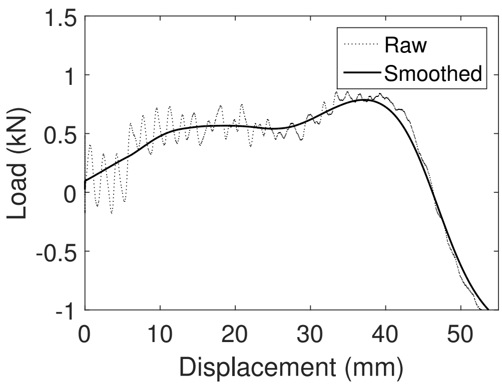

Figure B1: Impact testing force-displacement data before and after smoothing

Table B1 summarises the important impact testing results obtained.

Specimen	a_m **(g)**	a_p **(g)**	e_k **(J)**
Ninjaflex A	21.4	60.1	0.0
	19.5	61.3	2.0
Ninjaflex B	15.2	27.5	9.8
	14.2	25.4	11.5
Foam	5.5	10.7	37.1
	4.8	9.9	39.1

Table B1: Deceleration and final kinetic energy for all impact tests